Evaluation of membrane fouling mitigation strategies in an algal membrane photobioreactor (AMPBR) treating secondary wastewater effluent

Luca Fortunato*, Andres Felipe Lamprea, TorOve Leiknes

Water Desalination and Reuse Center (WDRC), Division of Biological & Environmental Science & Engineering (BESE), 4700 King Abdullah University of Science and Technology (KAUST), Thuwal 23955-6900, Saudi Arabia

*Corresponding author: Tel. +966 12 808 2289; Email: Luca.Fortunato@kaust.edu.sa

Abstract

Microalgae-based advanced wastewater treatment has gained momentum due to the possibility of recovering nutrients for the production of fertilizers, biofuels and fine chemicals from microalgal biomass. The objective of this study is to evaluate the effect of different fouling control strategies on the development of *Chlorella vulgaris* in a membrane photobioreactor (AMPMBR) treating a secondary wastewater effluent. The experimental results showed a decrease in the fouling rate (bar/hours) of 50% for backwash and relaxation and 60% for nitrogen bubble scouring. Additionally, *in-situ* non-destructive real time monitoring was employed to visualize and assess the change in morphology of the algae formed on the membrane surface. The use of fouling mitigation led to substantial changes in the biomass morphologies impacting the performance of the AMPMBR. The lowest biomass deposition (5-10 μm) was

observed when nitrogen bubble scouring was employed, while the application of relaxation led to the thickest (180 μm), most heterogeneous and porous structure. The use of backwash led to a partial temporary biomass detachment from the membrane surface. This study, provided a better understanding of the impact of fouling mitigation strategies on the biomass formed on the membrane of AMPMBR.

Keywords: Algae Growth; Relaxation; Backwash; Scouring; MBR; OCT;

1. Introduction

The use of microalgae has been proposed as an energy and cost-efficient alternative to tackle the global water and energy challenges (Arashiro et al., 2018; Solimeno and García, 2017). A cost-efficient supply of nutrients and water can be achieved by using wastewater as the media for algae feedstock production, whereas the algal biomass can be used to improve the wastewater effluent quality, removing nitrogen and phosphorous (Khiewwijit et al., 2018; López-Serna et al., 2019). The algal biomass produced could be transformed in valuable byproducts such as biofuels, fertilizers and fine chemicals. Nevertheless, the separation of algal biomass from the water is considered a major technical and economical challenge (Gutiérrez-Alfaro et al., 2018). Among the algal separation technologies, the use of membrane filtration has gained momentum due to its cost and energy efficiency (Luo et al., 2017).

An inherent phenomenon in membrane filtration is membrane fouling which causes a subsequent permeate flux decline, and represents one of the main bottlenecks for widespread application of membrane photobioreactors (MPBR) in water treatment and algal cultivation. Over time, membrane fouling leads to reduced membrane permeability due to the accumulation of algal cells and their metabolic products on the membrane surface (Zhao et al., 2017). This process challenge has hampered large-scale commercialization of MPBRs (Castaing et al., 2011; Liang and Hu, 2012; Morineau-Thomas et al., 2002).

Ahmad et al. (2012), during the crossflow microfiltration of algae biomass observed

53 the prevalence of a pore blocking as main fouling mechanism at the early filtration
54 stage. The size of the microalgae cells in an APMBR varies, ranging from a few
55 micrometers to hundred micrometers (Zhang et al., 2010), and the fouling formed is
56 mainly due to cake layer formation (Castaing et al., 2010; Morineau-Thomas et al.,
57 2002), although the contribution of the cake layer to the hydraulic resistance is lower
58 compared to other processes (Lee et al., 2001).
59
60 Different membrane fouling control strategies have been proposed to mitigate the
61 biomass deposition on the membrane surface over the time (Bilad et al., 2014). The
62 most widely used strategies include an operational approach where loading rates,
63 subcritical flux conditions are applied; additionally physical fouling controls such as
64 backwash, membrane relaxation and air scouring are commonly employed to remove
65 or reduce fouling development (Eliseus et al., 2017; Zhang and Fu, 2018). Membrane
66 fouling cannot be completely avoided, and these techniques are considered
67 preventive actions capable of reducing the fouling effects and thus enhance the
68 overall system performance. However, the effectiveness of each control strategies
69 relies on different environmental and operating conditions. Furthermore, the
70 application of an inadequate control strategy can lead to a significant increase in
71 energy, and to a decrease in the quantity and quality of the permeate produced ,
72 decreasing the overall process performance (Zhou et al., 2015).
73
74 The mechanisms of the aforementioned strategies in the fouling mitigation, as well as
75 their impact on the biomass properties, are still not completely clear. Therefore, a

deeper understanding of the antifouling strategies, fouling mechanisms, and their interactions is critically important for the development of new alternatives in the future. This knowledge is particularly relevant in order to improve the economic and environmental performance of the process and to facilitate the widespread application of a novel and promising technology for the advanced wastewater treatment and algal production.

In this study, the impact of different membrane fouling control strategies was investigated. An algal hollow fiber membrane photobioreactor was used to study the growth and membrane attachment of *Chlorella vulgaris* in an AMPMBR process. The effect of relaxation, backwash and nitrogen scouring on controlling the biomass formed in membrane reactor was assessed. The fouling rate was normalized for the filtration time and the amount of permeate produced. The algal fouling layer that developed on the hollow fiber membrane was monitored in real-time through *in-situ* non-destructive observation performed with Optical Coherence Tomography (OCT). A new insight into the mechanism of each fouling control strategy is provided.

2. Materials and methods

2.1. Algae inoculum and pre-cultivation

The microalgae *Chlorella vulgaris* (UTEX 259) used in this study was purchased from UTEX Culture Collection of Algae (US). The seed was pre-cultivated autotrophically in Modified Bold's Basal Medium (BBM) purchased from Sigma-Aldrich. An algal seed from a running photobioreactor with the same media characteristics and growing conditions was employed for the experiments. The cells were initially cultured under batch mode in an incubation chamber with the addition of sodium bicarbonate ($NaHCO_3$) to the medium as inorganic carbon source (750 mg/L). More detailed information can be found elsewhere (Najm et al., 2017).

2.2. Experimental setup

A customized cylindrical glass airlift photobioreactor with a total volume of 2.5 L (working volume of 2.0 L) was used for the study, with a surface to volume ratio of the reactor of 13.7. The reactor was illuminated continuously with white LED illumination at a photosynthetic photon flux density (PPFD) of 130 μmol photons/m_2/s. The algal reactor was continuously operated with a synthetic secondary wastewater feed with no organic carbon source and total nitrogen and dissolved inorganic phosphorous concentrations of 60 and 10 mg/L, respectively (Table 1). Compressed air was the sole source of inorganic carbon; it was passed

through a 0.2 μm filter and then bubbled with air diffusers into the reactor at a rate of 30 L/h. The temperature was kept at 25°C, and the pH was daily monitored and kept between 7 and 8 using sodium bicarbonate ($NaHCO_3$) (Mohd Udaiyappan et al., 2017). The solution was provided by means of a peristatic pump (Masterflex ®, Cole-Parmer, United States) and the liquid level in the reactor was maintained constant by using a level controller (Fig. 1). The as-grown *C. vulgaris* cell suspension was continuously fed into an automatic filtration unit (Osmo Inspector ™, Convergence, The Netherlands) where a hollow fiber module was used to uninterruptedly extract the permeate. The cell suspension was circulated through the membrane filtration unit at a speed of 2 L/h. The permeate was extracted and collected in a pre-weighted tank, whereas the retentate was continuously recirculated back into the photo reactor, both operations carried out by pumps incorporated in the filtration unit. (Fig. 1)

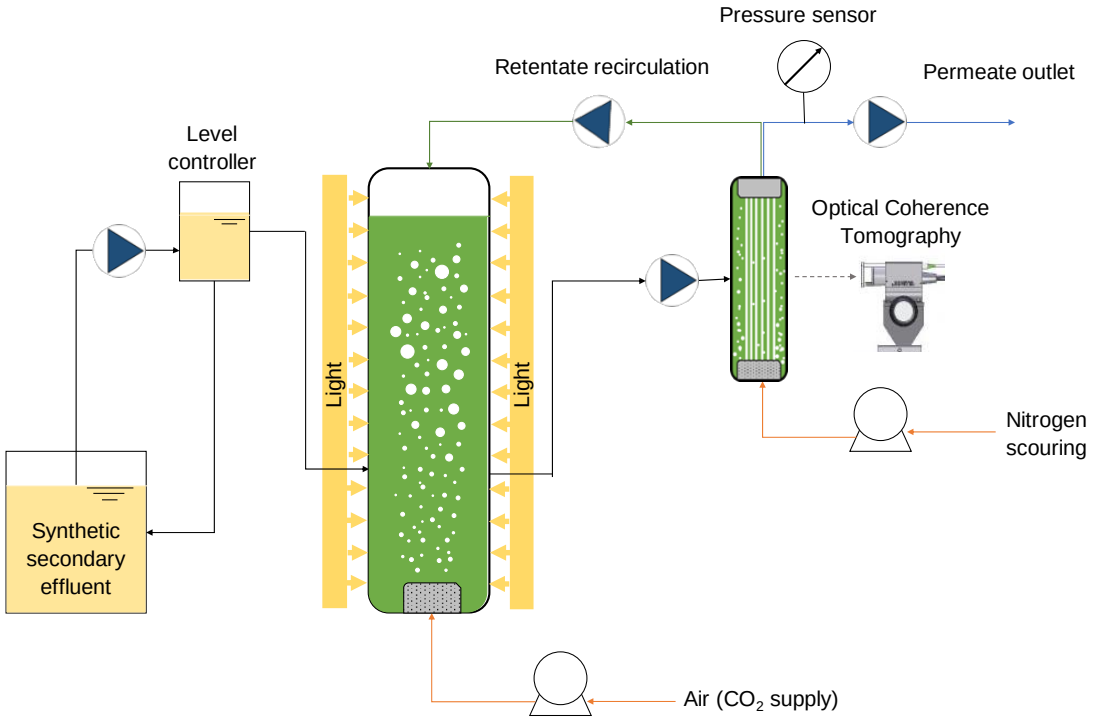

128

129 **Fig. 1.** Representation of the experimental setup. *In-situ* monitoring with Optical
130 Coherence Tomography (OCT) was performed directly in the algae photo membrane
131 bioreactor (APMBR) setup.

132

133 The system was acclimatized for a period of 120 days under the specified conditions
134 before the start of the experiments. The algal concentration in the reactor was
135 adjusted to 500 mg/L during the last 10 days of operation at HRT 12 h. The biomass
136 trend during the latter period prior the experiment is shown in Fig S1. The membrane
137 filtration unit as operated with a constant flux of 20 LMH. The membrane filtration
138 module was constructed with PVDF hollow fiber membranes (GE$_{TM}$, USA), with
139 specifications given in Table S1. The water permeability was determined in the
140 laboratory by filtering DI water and measuring the TMP profile. The pore size was

141 determined by Field Emission Scanning Electron Microscopy (FESEM).

142

143 Table 1. Composition of the synthetic wastewater.
144

Compounds	Concentration (mg/L)
NH_4Cl	230.00
KH_2PO_4	44.00
$MgSO_4 \cdot 7H_2O$	3.75
$CaCl_2 \cdot 2H_2O$	1.80
EDTA	0.50
$FeSO_4 \cdot 7H_2O$	0.40
$MnCl_2 \cdot 4H_2O$	1.80
$ZnSO_4 \cdot 7H_2O$	0.22
$NaMoO_4 \cdot 5H_2O$	0.39
$CoCl_2 \cdot 6H_2O$	0.41

145

146 **2.3. Fouling control experiments**

147 The effects of three physical membrane fouling control strategies were investigated,
148 relaxation, backwash and nitrogen scouring,. All experiments were performed by
149 applying cycles of 20 minutes of membrane filtration followed by 10 minutes of the
150 physical fouling control. No permeation took place during the fouling control cycles
151 providing a total filtration time of 120 minutes and an effective permeation time of
152 80 minutes. For the backwash cycles ($APMBR_{BW}$), a backwash flux of 25 LMH was
153 continuously supplied during 10 minutes control period (Shekhar et al., 2017). For
154 the scouring strategy ($APMBR_{SC}$), compressed pure nitrogen gas was bubbled
155 continuously through a diffuser into the reactor at a rate of 2.22 L/h for the 10
156 minutes period of each cycle (Javadi et al., 2014; Zhang and Fu, 2018). For relaxation
157 ($APMBR_{RLX}$), permeation and recirculation in the filtration module was stopped. A
158 continuous filtration mode, without any fouling mitigation strategies applied, was

operated as a control ($APMBR_{CT}$).

2.4. Fouling assessment

The fouling propensity of the APMBR operated under the specified experimental conditions was assessed by measuring the transmembrane pressure (TMP) increase over time. The fouling rates were normalized by the increase in TMP for the effective permeation time and expressed as bar/hours. Moreover, the fouling rates were also calculated by taking into account the volume of permeate produced for each run (taking into account the amount of permeate used for backwashing), by dividing the TMP for the liter of permeate produced, and expressed as bar/L of permeate.

2.5 Biomass characterization

The microalgae concentration was determined using the optical density of the microalgae culture at 680 nm (OD_{680}) with a UV spectrophotometer (DR 2500, Hach®, United States). Particle size distribution of biomass suspensions were analyzed by triplicates using a laser diffraction particle analyzer (Master Sizer Macro ™, Malvern, UK), applying a refractive index (n) for Chlorella of 1.086, and water as dispersant (n=1.33) at an obscuration of 18%. Samples were collected in the Osmo Inspector ™ filtration cell during and after the physical cleaning cycle for each control strategy.

2.6. In situ monitoring

An optical coherence tomography unit (OCT, Thorlabs GANYMEDE spectral domain OCT system with a central wavelength of 930, Thorlabs, GmbH, Dachau, Germany)

equipped with a 5X telecentric scan lens (Thorlabs LSM 03BB) was used to investigate the formation and growth of the algal biomass on the submerged hollow fiber membrane filtration unit. The OCT probe was fixed to a motorized frame (Velmex, USA) in order to allow the movement in a system of 3D coordinates (Fortunato et al., 2016). The 2D cross section scans (1666 x 680 pixel) corresponding to 5.0 x 1.4 mm (width x depth) were taken within a fixed rectangular position of 5.0 x 0.5 mm during all the experiments. For the analysis of the images, the OCT scans were preprocessed using FiJi software. A multi-sequence step was applied: 1) the images were filtered: 2) contrast and brightness were adjusted and, 3) the images were thresholded and binarized. This was followed by the calculation of the thickness and roughness of the algal biofilm formed on the membrane surface using a customized MATLAB code (Fortunato et al., 2017b). Each pixel corresponds to a certain length related to the setting acquisition (lateral resolution 8 μm and axial resolution 4.2 μm). The mean algal biofilm layer thickness (Z in μm) and the relative roughness coefficient (R'a) were calculated according to the equations reported in literature (Fortunato et al., 2017c).

The signal ratio (SR) was measured to assess the change in biomass proprieties, defined as the ratio between the average biomass intensity pixels (Bi) and the average background intensity pixels (Ni).

$$SR = \frac{< Bi >}{< Ni >} \quad (1)$$

The SR was used for the first time to assess the optical density of the cake layer related

205 to the density of the biomass deposited on the membrane surface.

206 For visualization purpose a look up table (LUT) color was applied to the OCT images.

3. Results and Discussion

3.1 Fouling development in the APMBR

In this study, the fouling propensity of the algae membrane photobioreactor operated under constant flux was assessed by measuring the TMP over time. TMP results for the three control strategies are presented for the total operating time and normalized by expressing the change as function of permeation time (Fig. 2).

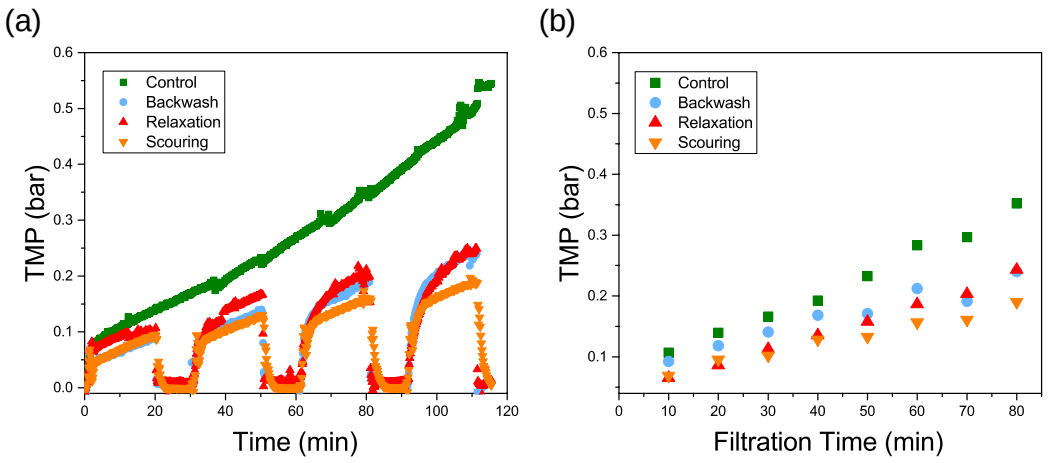

Fig. 2. TMP development vs total operation time (a), and vs filtration time (b). In the latter the TMP values were normalized for the effective time of permeation taking into account only the filtration cycles.

The comparative TMP profiles across the experiments are presented in Fig. 2. As expected, the highest fouling rate was observed in the control experiment (APMBR$_{CT}$) where no fouling mitigation strategy was employed. A TMP of 0.35 Bar was observed after 80 minutes operation and 0.50 Bar after 110 minutes of operation. The TMP measurements for the three strategies tested confirm the positive effect of the

224 physical cleaning strategies as a means to mitigate the membrane fouling, with a
225 reduction in the fouling rate of 50% for backwash and relaxation and of 60% for
226 nitrogen scouring, when compared to the control experiment.
227
228 For the three control strategies investigated, the lowest fouling rate was observed
229 for the bubble scouring ($APMBR_{SC}$) while backwash ($APMBR_{BW}$) and relaxation
230 ($APMBR_{RLX}$) presented similar fouling rates. However, the fouling rate expressed as
231 TMP vs. filtration time should not be used as the sole indicator to assess the
232 effectiveness of the control strategy. Backwash, scouring and relaxation are
233 characterized by different action mechanisms, involving higher or no consumption of
234 energy and permeate. The backwash procedure consists of applying a permeate
235 backflow through the membrane pores and the amount of permeate used reduces the
236 net water production of an installation and thus, depending on the minimum
237 backwash flow rate required to remove the foulants attached to the membrane
238 surface, the net performance of a filtration system can be considerably reduced. In
239 contrast, relaxation aims to remove the foulant by stopping the permeate suction and
240 therefore the convective drag force towards the membrane surface, facilitating the
241 back diffusion-induced detachment of different foulant agents (Eliseus et al., 2017;
242 Rickman et al., 2012) . The loss of productivity due to the use of permeate during the
243 backwash cycle is not always considered when studying the effect of the control
244 strategies (Judd, 2008). To compare the strategies investigated the TMP was
245 normalized for the net permeate production.
246

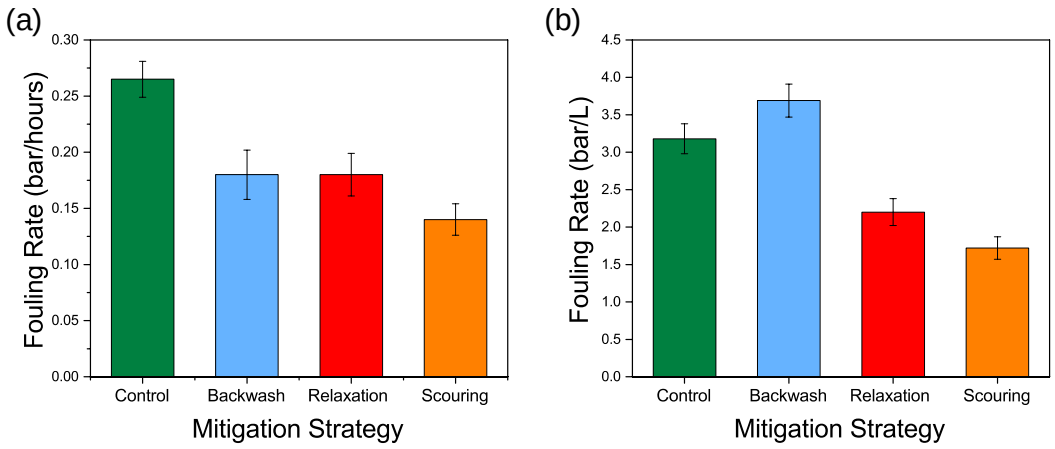

247

248 **Fig. 3**. Fouling rates under different fouling mitigation strategies. The fouling rates
249 were normalized for the effective filtration time (a) and the permeate produced (b).

250

251 As shown in Fig. 3, although APMBR$_{RLX}$ and APMBR$_{BW}$ show similar fouling rates
252 when expressed per total filtration time (0.18 Bar/hr), a significant difference can be
253 seen when the fouling rates are normalized for the permeate produced (3.7 vs. 2.2
254 Bar/L). The APMBR$_{BW}$ strategy presented the highest fouling rate for the normalized
255 TMP. In a full-scale operating plant these parameters become critical for the economic
256 viability of the process as backwash is a permeate and energy demanding process
257 when used as a fouling mitigation strategy. For tests conducted in this study,
258 operating the reactors with a biomass concentration of 500 mg/L and a flux of 20
259 LMH, the APMBR$_{RLX}$ and APMBR$_{BW}$ showed a similar TMP development after four
260 filtration cycles corresponding to 80 min of effective permeation. However, the latter
261 control strategy results in a lower net permeate production.

262

263 **3.2 *In-situ* monitoring of Algae formation**

OCT was applied as an *in-situ* monitoring tool to provide a better understating of the behavior and fouling control mechanism of the strategies applied. This work represents the first attempt to monitor *in-situ* and noninvasively the effect of different fouling mitigation approaches on algal biomass formed on a submerged membrane during filtration. The technique enables providing real-time information of the evolution and change in biomass morphology as a function of time and strategy used. Changes in morphology during operation were evaluated at different time intervals.

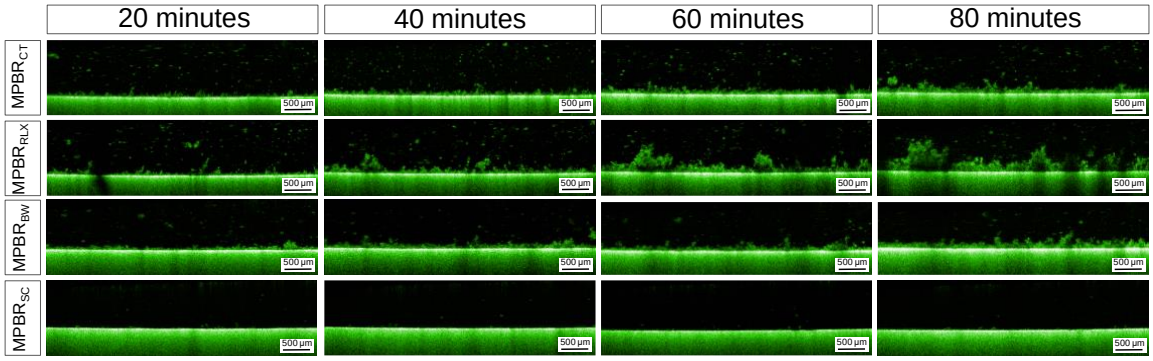

Fig. 4. Evolution of the algae biomass morphology over the time under different fouling mitigation strategies in algae photo membrane bioreactor (APMBR).

A time series for each of the strategies tested are shown in Fig. 4. A considerable difference in terms of biomass formed on the hollow fiber membrane was only observed for the bubble scouring (APMBR$_{SC}$) as control strategy compared to the other modes of operation (APMBR$_{CT}$, APMBR$_{RLX}$, APMBR$_{BW}$). Image scans corresponding to the nitrogen bubble scouring mode of operation (APMBR$_{SC}$) show a significantly lower amount of algae deposited on the membrane surface. Fig. 5 shows representative results of the fouling layer developed at the end of the observation period for the different modes of operation tested, where significant differences in

the biomass morphology and structure are readily apparent.

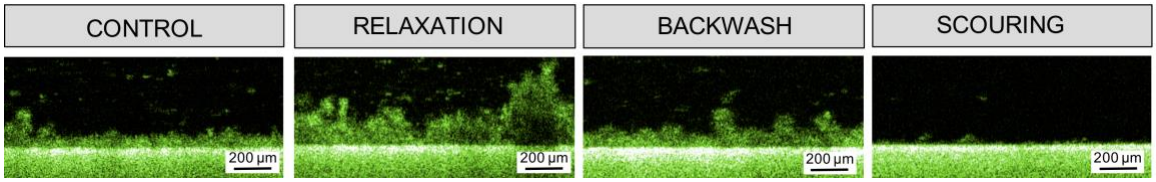

Fig. 5. Cropped 2D OCT cross sectional scans of the of the algae biomass morphology deposited on the membrane surface after 80 minutes of effective filtration employing different fouling mitigation strategies.

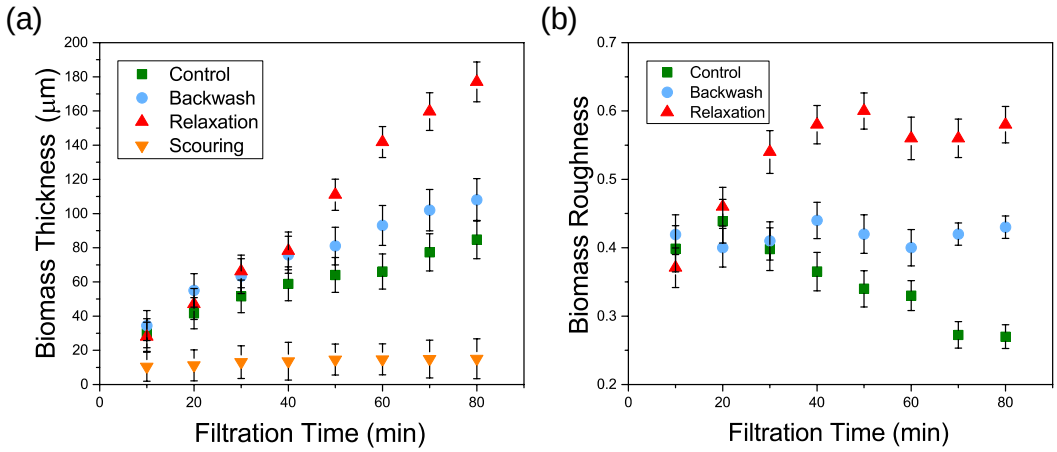

Fig. 6. Characterization of the algae morphology over the time deposited on the membrane surface through OCT scans image analysis. Algae biomass thickness (a) and algal biomass roughness (b).

Captured OCT images can be used to visualize the biomass structure at a given time and extract structural properties, thus enabling monitoring and quantifying changes over a time period (Fortunato et al., 2019, 2018). Table 2 shows the biomass

298 descriptors after 80 minutes of permeation. From the OCT scans the average algae
299 thickness over the time for each run was evaluated, with results presented in Fig. 6A.
300 For the APMBR$_{SC}$ strategy a minimum and constant value of 5-10 μm thickness was
301 observed for the whole period of monitored (close to the detection limit range of ~4
302 μm). During the first 40 min of operation, a constant and similar increase in the
303 average algal layer thickness was observed for the APMBR$_{CT}$, APMBR$_{BW}$ and
304 APMBR$_{RLX}$ strategies with values of 20 μm, 25 μm and 26 μm respectively. After 50
305 min operation, a sharper and growing difference in the biomass thickness was
306 observed for the different runs. At the end of the experiment the highest algae
307 thickness was observed for the APMBR$_{RLX}$ (180 μm), followed by the APMBR$_{BW}$ (108
308 μm) and APMPBR$_{CT}$ (85 μm) (Fig. 6 and Table 2). A similar trend was observed for the
309 biomass roughness, with the highest value for APMBR$_{RLX}$ (0.58), followed by the
310 APMBR$_{BW}$ (0.43) and APMPBR$_{CT}$ (0.27). The behavior of the biomass formed with no
311 control strategy (APMPBR$_{CT}$) is in agreement with results reported in previous
312 studies on membrane performance without applying physical cleaning showing a
313 decrease in roughness and a tendency towards more compact and dense morphology
314 at early stages (Pathak et al., 2018; Wang et al., 2017). A different trend was found for
315 the APMBR$_{BW}$ and APMBR$_{RLX}$, showing a constant and higher value in relative
316 roughness during the whole period of observation.
317 The data analyzed from the OCT scans demonstrate that the different membrane
318 fouling mitigation strategies led to different algal film morphologies over time.
319 APMBR$_{RLX}$ and APMBR$_{BW}$ showed a similar value of TMP (Fig. 2) while presenting
320 different morphology whereas the highest thickness and roughness were found for

321 APMBR$_{RLX}$. Indeed, the morphology of biomass deposited on the membrane directly
322 impacts the filtration efficiency, however the algal biomass thickness is not the only
323 morphological parameter that correlates to the membrane performance decrease (i.e.
324 TMP increase or flux decrease) and the impact on the hydraulic resistance caused.
325 Another parameter found to correlate to the filtration performance is the biomass
326 roughness. Previous studies showed that the biofilm roughness developed on a UF
327 membrane has a positive impact on the permeate flux (Fortunato et al., 2017c; Peter-
328 Varbanets et al., 2012). Therefore, the algal biomass developed under APMBR$_{RLX}$
329 although presented the highest thickest, resulted to be more irregular and less dense
330 compared to the other cases, showing a similar hydraulic resistance compared to
331 thinner and more regular biomass developed under backwash. Hence, for APMBR$_{RLX}$
332 the "negative" effect of higher thickness on the hydraulic resistance was balanced by
333 the "positive" effect of a more irregular and heterogenous morphology.
334 Moreover, in this study the OCT images were used for the first time to try to assess
335 the difference in the "density" of the biomass layer formed on the membrane. By
336 measuring the ratio between the biomass pixels intensity and the background pixels
337 intensity it is possible to assess the cake layer density. After 80 min of filtration, the
338 intensity ratio for the APMBR$_{CT}$, APMBR$_{BW}$ and APMBR$_{RLX}$ modes of operation were
339 1.10, 1.11 and 1.20 respectively (Fig. 7). Results indicate that a biomass with a higher
340 signal intensity corresponded to a denser structure, leading to higher hydraulic
341 resistance. The trend was found to be inversely proportional to the cake layer
342 thickness.
343 In summary, by analyzing the TMP behavior and the algal biomass cake layer

morphology, it is clear that the different control strategies used had different effects and impacts on the biomass morphology and thus the hydraulic resistance of the algal biomass deposited on the membrane surface.

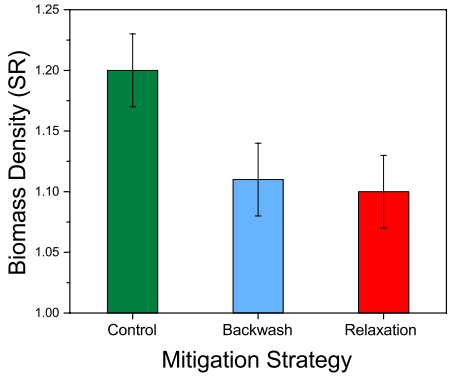

Fig. 7. Signal ratio (SR) after 80 min of filtration for the biomass developed under different fouling control strategies. The SR was calculated from OCT scans and employed to assess the difference in biomass density by using different fouling mitigation strategies.

Table 2. Membrane performance and algal biomass characterization after 80 minutes of effective permeation.

	TMP	Average Thickness (µm)	Relative Roughness	Biomass Density (SR)
Control	0.35	85±11	0.27±0.02	1.20±0.03
Backwash	0.24	108±12	0.43±0.02	1.11±0.03
Relaxation	0.24	180±12	0.58±0.03	1.10±0.03
Scouring	0.19	10*	-	-

*The algal biomass formed on the membrane surface when using nitrogen scouring was close to the OCT detection limit. Therefore, was not possible to perform a detail morphology analysis for the scouring.

3.3 Assessing the impact of different fouling mitigation strategies

360 Experiments were conducted in a filtration cycle consisting of two stages: (i) 20 min
361 of filtration (i.e. deposition of biomass), (ii) followed by 10 min of biomass control
362 without permeation. The control strategy has a double effect on the algae deposited
363 in the system affecting both the morphology of the biomass deposited on the
364 membrane and the biomass present in the feed. In this study, the OCT was employed
365 to study the behavior during the control mechanism cycle of action. By changing the
366 acquisition scan frequency, it was possible to generate time series of the response of
367 the biomass during each cycle of action. Moreover, the feed before and after the cycle
368 was analyzed by collecting samples from the reactor to evaluate the effect of the cycle
369 on the feed. The proposed approach allowed getting an insight of the effect of the
370 control strategies on the algae formed on the membrane.
371
372 **3.3.1 Backwashing**
373 Operation of membrane filtration systems with backwashing requires extra energy
374 and water (*i.e.* permeate) for backflow through the membrane. In this study, the
375 backwash mode of operation ($APMBR_{BW}$) did not show any significant enhancement
376 in filtration performance compared to relaxation ($APMBR_{RLX}$) (Fig. 2). Backwashing
377 has been reported to have an adverse effect on filtration performance, where frequent
378 backwashing was reported to induce macromolecules entering the membrane pores,
379 changing the fouling layer composition, and increasing the percentage of irreversible
380 fouling after the first cycles of operation (Wu et al., 2008). Backwashing was reported
381 to cause cake layer detachment leading to an increase in the soluble microbial
382 product (SMP) fraction which correlated to a higher degree of membrane fouling

383 (Metzger et al., 2007).

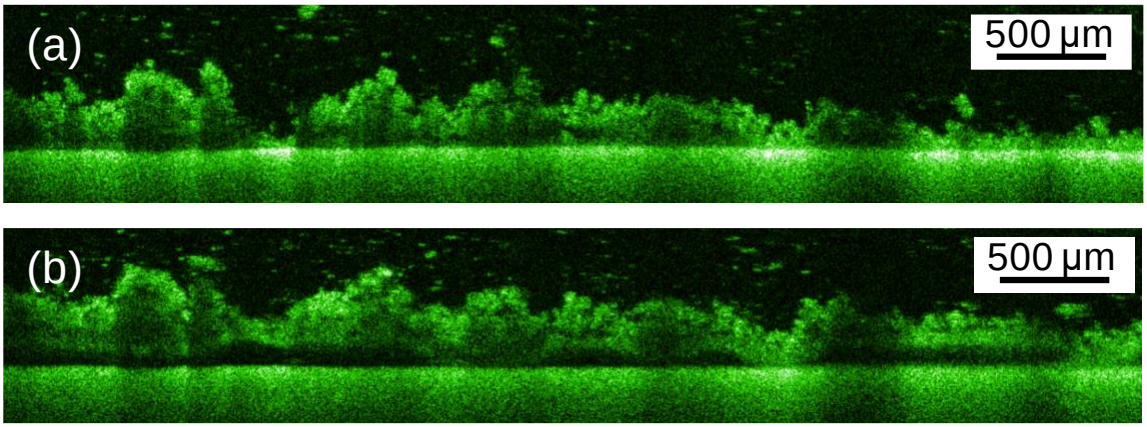

384

385 **Fig. 8.** 2D cross sectional scans of the algae biomass deposited on the membrane
386 during the backwash cycle. (a) before and (b) during backwash.

387

388 In this study, the partial detachment of the biomass from the membrane during the
389 backwashing was observed (Fig. 8). Video 1 (supplementary material) shows a
390 change in the membrane morphology observed during the backwash. Different stages
391 can be seen; (i) the biomass first relaxes (*i.e.* expands a little), (ii) then partially
392 detaches from the membrane, (iii) then redeposits on the membrane. The partial
393 detachment results in a reversible behavior where the algae biomass once detached
394 returns to the membrane surface when the backwash cycle ends. The detachment is
395 not complete, where portions of the cake layer (~ 50 µm wide) act as anchor points
396 for the biomass (Fig. 8). A similar behavior was reported by Shao et al. (Shao et al.,
397 2018) in a study on the effect of backwash on biofouling mitigation in ultrafiltration.
398 In contrast to assumptions made by Metzger et al. (2007), the backwash as conducted
399 in this study did not lead to a complete detachment of the biomass, suggesting that
400 backflow rate and pressure applied were not sufficient to reach a complete

401 detachment of the cake layer. This change in driving force created led to a partial
402 detachment of the algal biomass layer, lifting it about 150 μm from the membrane
403 surface. This temporary detachment of the biomass layer exposes the membrane
404 allowing smaller particles to reach the membrane surface and which are responsible
405 for the higher fouling propensity.
406
407 During a 10 min backwash cycle, in addition to the detachment of the algal biomass
408 layer removal of some particles from the biomass layer to the feed can be seen (Video
409 1 , supplementary material). This visual observation is confirmed by analysis of the
410 reactor supernatant where an increase in algae concentration and particle size
411 distribution (PSD) was measured after backwashing (Fig. S2A and S2B). These
412 findings are in agreement with results reported in the literature (Wu et al., 2008).
413
414 **3.3.2 Relaxation**
415 Of the fouling mitigation strategies investigated, relaxation is the less energy
416 intensive since as it simply consists in stopping filtration (*i.e.* permeation) for a
417 certain amount of time. In this study, the APMBR$_{RLX}$ operation was observed to have
418 a similar effect on the performance in terms of fouling rate (expressed in bar/hours)
419 compared to APMBR$_{BW}$ (Fig. 2). A significant difference in the biomass morphology
420 was observed between the APMBR$_{RLX}$ and APMBR$_{CT}$ modes of operation (Fig. 5-6). In
421 the absence of permeation (*i.e.* no convective forces towards the membrane) a
422 redistribution of the foulants present in the cake layer appears to take place. The
423 biomass behavior during relaxation was monitored by recording a taking video (

Video 2, supplementary material). During the relaxation cycle the algal biomass deposited on the membrane surface can be seen to responded to the change in the hydrodynamic conditions becoming less compressed and thus thicker, confirming the high compressibility of *Chlorella* cake layers reported in the literature (Babel and Takizawa, 2010). The *in-situ* observation conducted in this study confirms previously reported results found in biofilm studies where relaxation led to a more porous and less attached biofouling layer (Fortunato et al., 2017a; Peter-Varbanets et al., 2012; Valladares Linares et al., 2015). The morphology changes occurring within each relaxation cycle gradually affects the algal biomass structure over time. After four cycles, the deposited algal biomass becomes thicker with a higher roughness and looser structure (SR value) (Fig. 6-7). Analysis of the feed side show no significant changes particle sizes (*i.e.* PSD) or algae concentrations. The relaxation mode of operation appears to be effective in affecting the physical proprieties of the biomass layer formed, developing towards a looser and more irregular structure that leads to lower hydraulic resistance.

3.3.3 Scouring

Air scouring is the most commonly applied fouling control strategy in commercial MBR processes, however, this component of the system is energy demanding and represents one of the major items contributing to operational costs. Using large bubbles for scouring in submerged membrane configurations reduces the cake layer deposited on the membrane surface by inducing a non-homogeneous distribution of

447 air bubbles along the membrane surface, resulting in localized tubular and high shear
448 conditions. Although scouring reduces fouling it cannot prevent all the irreversible
449 fouling caused by small particles and AOM (Drexler and Yeh, 2014; Kanchanatip et al.,
450 2016).
451
452 In this study, the detailed time-resolved imaging during the scouring cycle was
453 limited by the presence of gas bubbles and the continuous movement of the
454 membrane that hindered the real-time monitoring (Fig. S3). Two scouring
455 mechanisms appear to be the most important: i) drag forces induced by the gas
456 bubbles shear off some of the foulants and ii) the membrane vibrations lead to
457 additional shear forces contributing to the detachment of the foulants (Bilad et al.,
458 2013; Cui et al., 2003).
459
460 As shown in Fig. 5, no significant deposition or buildup of algal biomass with scouring
461 can be observed, with only a thin layer of algae detectible with an average thickness
462 of 5-10 μm, close to the OCT resolution limit. Similar values in cake layer thickness
463 were reported in a study on the effect of air scouring intensity on hollow fibers in an
464 MBR process (Ye and Le-Clech, 2011). However, a TMP increase over the time was
465 found even with a consistent low algal biomass thickness, suggesting a different
466 fouling mechanism dominating the behavior compared to the other strategies tested.
467 Studies in the literature indicate that a cake layer formed on the membrane surface
468 of APMBR prevents further pore blockage and fouling providing an additional
469 filtration layer (Meng and Liu, 2013). For APMBRSC operation, the absence of a thick

algae layer led to a higher deposition of small particles on the hollow fiber membrane which form a thinner but have a higher hydraulic resistance (Lee et al., 2001; Liang and Hu, 2012). Compared to the other three modes of operation tested, where the rise in TMP can be correlated to increasing amounts of biomass over time, the TMP increase for scouring is less related to changes in the cake layer morphologies

The scouring effects interact directly with the algal biomass deposited on the hollow fiber where parts of the biomass are sloughed off and dispersed into the reactor, breaking them in smaller fragments and affecting the characteristics of the bulk fluid on the feed side and increasing the amount of submicron particles and thus the fouling propensity (Castaing et al., 2010; Ivanovic and Leiknes, 2008; Ladner et al., 2010). During scouring the hydraulics of the reactor are affected, increasing the algae concentration and particulates due to the mixing induced by the gas bubbles. This affected the feed characteristics in the reactor, increasing the overall algae concentration and shift in the particle size composition partially contributing to the increase of TMP observed (Fig. S2A). The high shear forces generated by the gas bubbles are known to affect the proprieties of the biomass, breaking it into smaller fragments and cell debris due to the fragile structure of algae (Almomani et al., 2019; Castaing et al., 2011; Chiou et al., 2010; Qu et al., 2012). These particles are characterized by being smaller than the nominal membrane pore size which can lead to pore blocking (Zhang and Fu, 2018). Ladner et al. (2010) reported an increase in material with higher fouling propensity when algal biomass was exposed to shear conditions. In summary, gas scouring as a control strategy for fouling mitigation has

493 a double and contradicting effect. Although the scouring effect from gas bubbles is
494 capable of reducing the amount of biomass deposited as a cake layer on the
495 membrane surface it can also lead to an increase in algae concentrations and generate
496 more particulates fractions that are significant contributors to fouling.
497
498 **4. Conclusions**
499 This study evaluated the use of fouling mitigation strategies in the control of the
500 deposition of *Chlorella vulgaris* in AMPMBR treating secondary wastewater effluent.
501 The results presented in this study indicated that after four cycles of operation,
502 fouling mitigation strategies showed a positive impact with a reduction in the fouling
503 rate of 50% for backwash and relaxation and of 60% for nitrogen bubble scouring.
504 However, when expressed as TMP/liters of permeate, the backwash showed the
505 highest fouling rate. The use of fouling mitigation strategies affected the biomass
506 morphology formed on the membrane due to the different mechanisms of action.
507 After 80 minutes of filtration the highest algae deposition on the membrane surface
508 was observed for the relaxation run with an average thickness of 180 μm, however
509 the biomass presented a lower hydraulic resistance due to a looser and more
510 irregular structure. The use of nitrogen bubble scouring minimized the deposition of
511 algae over the time on the membrane surface with the formation of a thin algae film
512 layer of 5-10 μm. During the backwash cycle, the change of driving force led to a
513 partial biomass detachment from the surface with the increase of the percentage of
514 irreversible fouling. The approach presented in this study enables correlating the
515 TMP increase to the algae grown under different mitigation strategies. This could be

employed in real operation to evaluate and enhance the net production of permeate and algae biomass.

Acknowledgement

This study was supported by funding from King Abdullah University of Science and Technology (KAUST). The graphical abstract was created by Heno Hwang, scientific illustrator at King Abdullah University of Science and Technology (KAUST).

References

Ahmad, A.L., Mat Yasin, N.H., Derek, C.J.C., Lim, J.K., 2012. Crossflow microfiltration of microalgae biomass for biofuel production. Desalination 302, 65–70. doi:10.1016/J.DESAL.2012.06.026

Almomani, F., Al Ketife, A., Judd, S., Shurair, M., Bhosale, R.R., Znad, H., Tawalbeh, M., 2019. Impact of CO2 concentration and ambient conditions on microalgal growth and nutrient removal from wastewater by a photobioreactor. Sci. Total Environ. 662, 662–671. doi:10.1016/J.SCITOTENV.2019.01.144

Arashiro, L.T., Montero, N., Ferrer, I., Acién, F.G., Gómez, C., Garfí, M., 2018. Life cycle assessment of high rate algal ponds for wastewater treatment and resource recovery. Sci. Total Environ. 622–623, 1118–1130. doi:10.1016/J.SCITOTENV.2017.12.051

Babel, S., Takizawa, S., 2010. Microfiltration membrane fouling and cake behavior during algal filtration. Desalination 261, 46–51. doi:10.1016/J.DESAL.2010.05.038

Bilad, M.R., Arafat, H.A., Vankelecom, I.F.J., 2014. Membrane technology in microalgae cultivation and harvesting: A review. Biotechnol. Adv. 32, 1283–1300. doi:10.1016/J.BIOTECHADV.2014.07.008

Bilad, M.R., Discart, V., Vandamme, D., Foubert, I., Muylaert, K., Vankelecom, I.F.J., 2013. Harvesting microalgal biomass using a magnetically induced membrane vibration (MMV) system: Filtration performance and energy consumption. Bioresour. Technol. 138, 329–338. doi:10.1016/j.biortech.2013.03.175

Castaing, J.-B., Massé, A., Pontié, M., Séchet, V., Haure, J., Jaouen, P., 2010. Investigating submerged ultrafiltration (UF) and microfiltration (MF) membranes for seawater pre-treatment dedicated to total removal of undesirable micro-algae. Desalination 253, 71–77. doi:10.1016/J.DESAL.2009.11.031

Castaing, J.B., Massé, A., Séchet, V., Sabiri, N.-E., Pontié, M., Haure, J., Jaouen, P., 2011. Immersed hollow fibres microfiltration (MF) for removing undesirable micro-algae and protecting semi-closed aquaculture basins. Desalination 276, 386–

554 396. doi:10.1016/J.DESAL.2011.03.081
555 Chiou, Y.-T., Hsieh, M.-L., Yeh, H.-H., 2010. Effect of algal extracellular polymer
556 substances on UF membrane fouling. Desalination 250, 648–652.
557 doi:10.1016/j.desal.2008.02.043
558 Cui, Z.F., Chang, S., Fane, A.G., 2003. The use of gas bubbling to enhance membrane
559 processes. J. Memb. Sci. 221, 1–35. doi:10.1016/S0376-7388(03)00246-1
560 Drexler, I.L.C., Yeh, D.H., 2014. Membrane applications for microalgae cultivation
561 and harvesting: a review. Rev. Environ. Sci. Bio/Technology 13, 487–504.
562 doi:10.1007/s11157-014-9350-6
563 Eliseus, A., Bilad, M.R., Nordin, N.A.H.M., Putra, Z.A., Wirzal, M.D.H., 2017. Tilted
564 membrane panel: A new module concept to maximize the impact of air bubbles
565 for membrane fouling control in microalgae harvesting. Bioresour. Technol.
566 241, 661–668. doi:10.1016/J.BIORTECH.2017.05.175
567 Fortunato, L., Bucs, S., Linares, R.V., Cali, C., Vrouwenvelder, J.S., Leiknes, T., 2017a.
568 Spatially-resolved in-situ quantification of biofouling using optical coherence
569 tomography (OCT) and 3D image analysis in a spacer filled channel. J. Memb.
570 Sci. 524, 673–681. doi:10.1016/j.memsci.2016.11.052
571 Fortunato, L., Jeong, S., Leiknes, T., 2017b. Time-resolved monitoring of biofouling
572 development on a flat sheet membrane using optical coherence tomography.
573 Sci. Rep. 7, 15. doi:10.1038/s41598-017-00051-9
574 Fortunato, L., Jeong, S., Wang, Y., Behzad, A.R., Leiknes, T., 2016. Integrated approach
575 to characterize fouling on a flat sheet membrane gravity driven submerged
576 membrane bioreactor. Bioresour. Technol. 222, 335–343.
577 doi:10.1016/j.biortech.2016.09.127
578 Fortunato, L., Li, M., Cheng, T., Rehman, Z.U., Heidrich, W., Leiknes, T., 2019. Cake
579 layer characterization in Activated Sludge Membrane Bioreactors: Real-time
580 analysis. J. Memb. Sci. 578, 163–171. doi:10.1016/J.MEMSCI.2019.02.026
581 Fortunato, L., Pathak, N., Ur Rehman, Z., Shon, H., Leiknes, T., 2018. Real-time
582 monitoring of membrane fouling development during early stages of activated
583 sludge membrane bioreactor operation. Process Saf. Environ. Prot. 120, 313–
584 320. doi:10.1016/J.PSEP.2018.09.022

585 Fortunato, L., Qamar, A., Wang, Y., Jeong, S., Leiknes, T., 2017c. In-situ assessment of
586 biofilm formation in submerged membrane system using optical coherence
587 tomography and computational fluid dynamics. J. Memb. Sci. 521, 84–94.
588 doi:10.1016/j.memsci.2016.09.004
589 Gutiérrez-Alfaro, S., Rueda-Márquez, J.J., Perales, J.A., Manzano, M.A., 2018.
590 Combining sun-based technologies (microalgae and solar disinfection) for
591 urban wastewater regeneration. Sci. Total Environ. 619–620, 1049–1057.
592 doi:10.1016/J.SCITOTENV.2017.11.110
593 Ivanovic, I., Leiknes, T., 2008. Impact of aeration rates on particle colloidal fraction
594 in the biofilm membrane bioreactor (BF-MBR). Desalination 231, 182–190.
595 doi:10.1016/J.DESAL.2007.11.046
596 Javadi, N., Zokaee Ashtiani, F., Fouladitajar, A., Moosavi Zenooz, A., 2014.
597 Experimental studies and statistical analysis of membrane fouling behavior and
598 performance in microfiltration of microalgae by a gas sparging assisted process.
599 Bioresour. Technol. 162, 350–357. doi:10.1016/J.BIORTECH.2014.03.160
600 Judd, S., 2008. The status of membrane bioreactor technology. Trends Biotechnol.
601 26, 109–16. doi:10.1016/j.tibtech.2007.11.005
602 Kanchanatip, E., Su, B.-R., Tulaphol, S., Den, W., Grisdanurak, N., Kuo, C.-C., 2016.
603 Fouling characterization and control for harvesting microalgae Arthrospira
604 (Spirulina) maxima using a submerged, disc-type ultrafiltration membrane.
605 Bioresour. Technol. 209, 23–30. doi:10.1016/J.BIORTECH.2016.02.081
606 Khiewwijit, R., Rijnaarts, H., Temmink, H., Keesman, K.J., 2018. Glocal assessment of
607 integrated wastewater treatment and recovery concepts using partial
608 nitritation/Anammox and microalgae for environmental impacts. Sci. Total
609 Environ. 628–629, 74–84. doi:10.1016/J.SCITOTENV.2018.01.334
610 Ladner, D.A., Vardon, D.R., Clark, M.M., 2010. Effects of shear on microfiltration and
611 ultrafiltration fouling by marine bloom-forming algae. J. Memb. Sci. 356, 33–43.
612 doi:10.1016/J.MEMSCI.2010.03.024
613 Lee, J., Ahn, W.-Y.W.-Y., Lee, C.-H.C.-H., 2001. Comparison of the filtration
614 characteristics between attached and suspended growth microorganisms in
615 submerged membrane bioreactor. Water Res. 35, 2435–2445.

616 doi:10.1016/S0043-1354(00)00524-8
617 Liang, Z., Hu, Z., 2012. Start-up performance evaluation of submerged membrane
618 bioreactors using conventional activated sludge process and modified Luzack-
619 Ettinger process. J. Environ. Eng. (United States) 138, 932–939.
620 doi:10.1061/(ASCE)EE.1943-7870.0000559
621 López-Serna, R., Posadas, E., García-Encina, P.A., Muñoz, R., 2019. Removal of
622 contaminants of emerging concern from urban wastewater in novel algal-
623 bacterial photobioreactors. Sci. Total Environ. 662, 32–40.
624 doi:10.1016/J.SCITOTENV.2019.01.206
625 Luo, Y., Le-Clech, P., Henderson, R.K., 2017. Simultaneous microalgae cultivation and
626 wastewater treatment in submerged membrane photobioreactors: A review.
627 Algal Res. 24, 425–437. doi:10.1016/J.ALGAL.2016.10.026
628 Meng, S., Liu, Y., 2013. Alginate block fractions and their effects on membrane
629 fouling. Water Res. 47, 6618–6627. doi:10.1016/j.watres.2013.08.037
630 Metzger, U., Le-Clech, P., Stuetz, R.M.R.M., Frimmel, F.H.F.H., Chen, V., 2007.
631 Characterisation of polymeric fouling in membrane bioreactors and the effect of
632 different filtration modes. J. Memb. Sci. 301, 180–189.
633 doi:10.1016/j.memsci.2007.06.016
634 Mohd Udaiyappan, A.F., Abu Hasan, H., Takriff, M.S., Sheikh Abdullah, S.R., 2017. A
635 review of the potentials, challenges and current status of microalgae biomass
636 applications in industrial wastewater treatment. J. Water Process Eng. 20, 8–21.
637 doi:10.1016/J.JWPE.2017.09.006
638 Morineau-Thomas, O., Jaouen, P., Legentilhomme, P., 2002. The role of
639 exopolysaccharides in fouling phenomenon during ultrafiltration of microalgae
640 (Chlorellasp. and Porphyridium purpureum): advantage of a swirling decaying
641 flow. Bioprocess Biosyst. Eng. 25, 35–42. doi:10.1007/s00449-001-0278-1
642 Najm, Y., Jeong, S., Leiknes, T., 2017. Nutrient utilization and oxygen production by
643 Chlorella vulgaris in a hybrid membrane bioreactor and algal membrane
644 photobioreactor system. Bioresour. Technol. 237, 64–71.
645 doi:10.1016/J.BIORTECH.2017.02.057
646 Pathak, N., Fortunato, L., Li, S., Chekli, L., Phuntsho, S., Ghaffour, N., Leiknes, T.O.,

Shon, H.K., 2018. Evaluating the effect of different draw solutes in a baffled osmotic membrane bioreactor-microfiltration using optical coherence tomography with real wastewater. Bioresour. Technol. 263, 306–316. doi:10.1016/j.biortech.2018.04.123

Peter-Varbanets, M., Gujer, W., Pronk, W., 2012. Intermittent operation of ultra-low pressure ultrafiltration for decentralized drinking water treatment. Water Res. 46, 3272–82. doi:10.1016/j.watres.2012.03.020

Qu, F., Liang, H., Tian, J., Yu, H., Chen, Z., Li, G., 2012. Ultrafiltration (UF) membrane fouling caused by cyanobateria: Fouling effects of cells and extracellular organics matter (EOM). Desalination 293, 30–37. doi:10.1016/J.DESAL.2012.02.020

Rickman, M., Pellegrino, J., Davis, R., 2012. Fouling phenomena during membrane filtration of microalgae. J. Memb. Sci. 423–424, 33–42. doi:10.1016/J.MEMSCI.2012.07.013

Shao, S., Wang, Y., Shi, D., Zhang, X., Tang, C.Y., Liu, Z., Li, J., 2018. Biofouling in ultrafiltration process for drinking water treatment and its control by chlorinated-water and pure water backwashing. Sci. Total Environ. 644, 306–314. doi:10.1016/J.SCITOTENV.2018.06.220

Shekhar, M., Shriwastav, A., Bose, P., Hameed, S., 2017. Microfiltration of algae: Impact of algal species, backwashing mode and duration of filtration cycle. Algal Res. 23, 104–112. doi:10.1016/J.ALGAL.2017.01.013

Solimeno, A., García, J., 2017. Microalgae-bacteria models evolution: From microalgae steady-state to integrated microalgae-bacteria wastewater treatment models – A comparative review. Sci. Total Environ. 607–608, 1136–1150. doi:10.1016/J.SCITOTENV.2017.07.114

Valladares Linares, R., Wexler, A.D., Bucs, S.S., Dreszer, C., Zwijnenburg, A., Flemming, H.-C., Kruithof, J.C., Vrouwenvelder, J.S., 2015. Compaction and relaxation of biofilms. Desalin. Water Treat. 1–13. doi:10.1080/19443994.2015.1057036

Wang, Y., Fortunato, L., Jeong, S., Leiknes, T., 2017. Gravity-driven membrane system for secondary wastewater effluent treatment: Filtration performance and

fouling characterization. Sep. Purif. Technol. 184. doi:10.1016/j.seppur.2017.04.027

Wu, J., Le-Clech, P., Stuetz, R.M., Fane, A.G., Chen, V., 2008. Effects of relaxation and backwashing conditions on fouling in membrane bioreactor. J. Memb. Sci. 324, 26–32. doi:10.1016/j.memsci.2008.06.057

Ye, Y., Le-Clech, P., 2011. Evolution of fouling deposition and removal on hollow fibre membrane during filtration with periodical backwash. Desalination 283, 198–205. doi:10.1016/J.DESAL.2011.03.087

Zhang, X., Hu, Q., Sommerfeld, M., Puruhito, E., Chen, Y., 2010. Harvesting algal biomass for biofuels using ultrafiltration membranes. Bioresour. Technol. 101, 5297–5304. doi:10.1016/j.biortech.2010.02.007

Zhang, Y., Fu, Q., 2018. Algal fouling of microfiltration and ultrafiltration membranes and control strategies: A review. Sep. Purif. Technol. 203, 193–208. doi:10.1016/j.seppur.2018.04.040

Zhao, F., Chu, H., Yu, Z., Jiang, S., Zhao, X., Zhou, X., Zhang, Y., 2017. The filtration and fouling performance of membranes with different pore sizes in algae harvesting. Sci. Total Environ. 587–588, 87–93. doi:10.1016/J.SCITOTENV.2017.02.035

Zhou, J., Wandera, D., Husson, S.M., 2015. Mechanisms and control of fouling during ultrafiltration of high strength wastewater without pretreatment. J. Memb. Sci. 488, 103–110. doi:10.1016/J.MEMSCI.2015.04.018